On the Parameterization and the Geometry of the Configuration Space of a Single Planar Robot

Technical Report

Dror Atariah Sunayana Ghosh Günter Rote

August 20, 2013

Contents

1 Introduction **3**
1.1 Definitions and Notations 4
1.2 Contacts and the Boundary of the Forbidden Space 7

2 Rotating the Robot **8**

3 Parameterizing Contact Surfaces **11**
3.1 Vertex-Edge Contact 11
3.1.1 Vertex Edge Angle Range Analysis 12
3.1.2 On the Exactness 14
3.2 Edge-Vertex Contact 14
3.2.1 Edge-Vertex Angle Range Analysis 15
3.2.2 Generalizing the Edge 16
3.3 Vertex-Vertex and Edge-Edge Contacts 17
3.3.1 Vertex-Vertex Contact 17
3.3.2 Edge-Edge Contact 18
3.4 Conclusion 18

4 Rational Parameterization **19**

5 Normals of the Contact Patches **20**

6 Differential Geometry of Contact Surfaces **21**
6.1 Geometrical Model 21
6.2 Rational Model 27

7 Conclusion **28**

A Angle Range Analysis Using Normals **28**
A.1 Vertex-Edge Case 29
A.2 Angle Range Analysis Using Normals - Edge-Vertex 31

B Differential Geometry of V-E Contact Surfaces **32**

Abstract

Translating and rotating planar polygonal robots are studied in the literature for decades. An integral part of this study is the configuration space which corresponds to the work space. In the context of motion planning problems, the boundary between the free and forbidden parts of the configuration space plays a major role. In this report we find an explicit parameterization of the boundary of the forbidden space. Using this parameterization we detail several geometrical properties of the various elements which constitute this boundary. In addition, this parameterization enables us to visualize these elements.

1 Introduction

The *piano movers problem* is about four decades old [20, 11] and studied intensively ever since. A fundamental part of this study is the configuration space which is associated to the work space at hand. A work space which consists of a planar polygonal convex robot, which is free to rotate and translate and polygonal obstacles give rise to a *configuration space*. Each point in the configuration space corresponds to a unique placement or pose of the robot in its work space, and vice versa, that is, every pose of the robot in the work space corresponds to a unique configuration point. The presence of obstacles in the work space translates to the partition of the configuration space into two parts, namely the *free* and *forbidden* spaces. Configuration points in the forbidden part correspond to poses in which the interior of the robot intersects the interior of one or more obstacles.

Most studies set the solution of the *motion planning problem* as the primary goal and thus focus mainly on algorithmical aspects. Thus, the related configuration space was hardly studied from a *geometrical point of view*. In this paper we focus on the geometrical properties of the configuration space which is associated to the piano movers problem. To that end, we derive in Section 3 an explicit parameterization of the boundary of the forbidden space. Better understanding of this boundary can contribute, for example, to the general study of the motion planning problem. In turn, using this parameterization we study in Section 6 the geometrical properties of this boundary.

In terms of visualization, most of the illustrations of the configuration space that can be found in the literature are rather simple. It is well known that for a robot which can *only* translate, the boundary of the forbidden space is polygonal and can be computed using *Minkowski sums*. Thus, most of the visualizations slice the configuration space with horizontal planes. Each slice corresponds to a fixed rotation of the robot and the boundary can be computed using Minkowski sums. Finally, stacking these slices yields a discrete visualization of the obstacles as they appear in the configuration space [12]. Using our parameterization it is easy to visualize the boundary of the forbidden space, as can be seen in Figure 12 and in [1].

Holonomic vs. non-holonomic. A robot for which *any* path in the configuration space is a valid motion in the work space (in the absence of obstacles) is called *omni-directional robot* or *holonomic*. On the other hand, if the robot is subject to velocity constrains, then both constrains and the robot called *non-holonomic*. For further details

consider [6, p. 10,48], [21, §7.3.1] and [13]. [27] describes a method which is designed for both holonomic and non-holonomic robot; however, it does not provide a general solution to neither of the settings. In this work we consider only the *holonomic* case, i.e. the controllable degrees of freedom equals the total degrees of freedom.

Previous work. The notion of configuration space was used for the first time in the seminal work of Lozano-Pérez and Wesley [15]. Surveys like [9, 26] can provide an overview at least on early related works. However, as we already pointed out, the literature aims mainly at the motion planning problem and hardly considers the boundary of the forbidden space per se, let alone parameterizing it or studying its geometrical properties.

Two interesting examples are [3, 17]. Both attempt to solve the motion planning problem itself, although they provide, as a byproduct, some idea on the geometrical nature of the boundary of the forbidden space. Yet, neither of them provides an explicit representation of the various elements of the boundary. Another interesting example is the work presented by Varadhan et al. [25] where the boundary between the forbidden and the free spaces is approximated. The approximation obtained is guaranteed to be topologically correct and within some prescribed Hausdorff distance from the actual boundary's surface. Again, this work does not provide any geometrical insight on the nature of neither the contact surfaces nor their geometry. In his work, Brost [4] obtains both geometrical and topological information on the configuration space. Yet again, the obtained description is not straightforward.

The literature in terms of visualization of the configuration space is rather limited. Based on the parameterization which is presented in this paper Atariah and Rote [1] presented a scientific video which visualizes the configuration space of a planar polygonal robot. The visualization presented in [22] gives another glimpse into a configuration space. In this case the boundaries of the robot and the obstacles comprise line segments and circular arcs.

Configuration spaces were considered also in slightly different contexts. For example, Bajaj and Kim [2] considered the case of a robot with *curved* boundary which translating amid similar obstacles. As we discuss later (cf. Section 1.1), the configuration space can be considered as a *group*. Lysenko, Nelaturi, and Shapiro [16] addressed the motion planning problem and other related problems as well using tools from *group morphology*. We conclude this paragraph with two more examples [23, 8] where the contact surfaces were considered.

1.1 Definitions and Notations

In this section we describe all the notations and notions that will be used throughout the paper. Further details can be found in standard textbooks like [21, 14, 6, 13]. In addition refer to Figure 1 for illustrations of the various definitions.

The robot. A robot A is a convex planar polygon with n vertices denoted by $\{a_i\}_{i=1}^{n}$; we assume that they are given in counterclockwise order. Throughout the paper, we

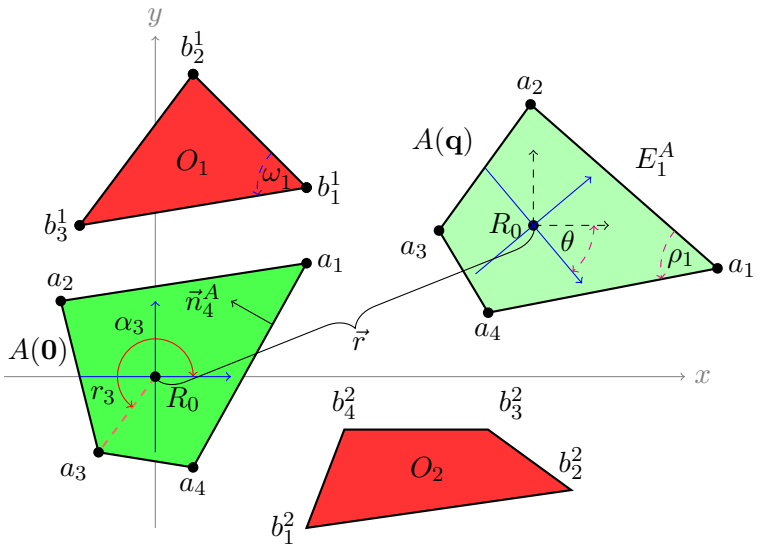

Figure 1: Work space example with the robot $A(\mathbf{0})$ in its rest position (dark green) and in a configuration resulting of a translation by a vector $\vec{r}$ and rotation in angle θ (light green), that is $A(\mathbf{q})$ where $\mathbf{q} = (\vec{r}, \theta)$.

follow the convention that $a_{n+1} = a_1$ and $a_0 = a_n$. The robot can translates and rotates in a *work space* scattered with polygonal (convex) obstacles. The work space is denoted by $\mathcal{W}$ and we take it to be $\mathcal{W} = \mathbb{R}^2$. The *reference point* of the robot is denoted by R_0, and we assume that in the *rest position* it is at the origin. Furthermore, we assume that the *local frame* of the robot aligns with the one of the work space when in the rest position. The vertices of the robot are either given with Cartesian coordinates, or with polar coordinates. For the vertex a_i we use the following notation $a_i = r_i\,(\cos\alpha_i, \sin\alpha_i)$ where $r_i := \|a_i\|$ and α_i denotes the angle with respect to the local frame of the robot. Finally, we assume that the vertices are in an increasing angular order, that is $0 \leq \alpha_1 \leq \ldots \leq \alpha_n < 2\pi$. The two assumptions, on the order of the vertices of the robot and the monotonicity of their angles, can lead to inconsistencies, as depicted in Figure 2. To avoid this, we assume, in addition, that the reference point lies in the interior or on the boundary of A. In the rest of the paper, we have that $a_{i-1} = a_n$ if $i = 1$, and similarly, $a_{i+1} = a_1$ if $i = n$. Finally, we denote by ρ_i the internal angle corresponding to the i-th vertex.

Obstacle(s). Let $\{O_k\}_{k=1}^m$ be m obstacles in the work space. The *vertices* of O_k for some k are given in counterclockwise order, and are denoted by $\{b_j^k\}$. We follow the same convention on the vertices of the obstacles, as we had for those of the robot. Finally, the interior angle at the j-th vertex will be denoted by ω_j^k. If the context introduces no confusion then we shall omit the index k. We adopt the same convention regarding the cyclic ordering of the vertices as we formalized for the vertices of the robot.

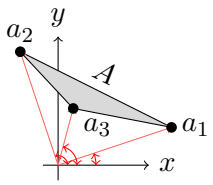

Figure 2: An example of a triangular robot whose vertices cannot be both counterclockwise ordered and in increasing angular order.

Edges and their normals. An *edge* (vector) $\overline{a_i a_{i+1}}$ of the robot connecting a_i to a_{i+1} is denoted by E_i^A; that is $E_i^A = a_{i+1} - a_i$. Similarly, the j-th edge (vector) of the obstacle O_k connecting b_j^k to b_{j+1}^k is $E_j^{O_k}$. The *(inward) normals* of the edges E_i^A and $E_i^{O_k}$ are denoted by $\vec{n}_i^A$ and $\vec{n}_j^{O_k}$ respectively. Note that according to the definition, the normals are not necessarily unit vectors.

Configuration space and poses. We let $\mathcal{C}$ denote the *configuration space* of the robot A in the work space $\mathcal{W}$ which is scattered with the obstacles $\{O_k\}$. The *free* and *forbidden* parts of $\mathcal{C}$ are denoted by $\mathcal{C}_{\text{free}}$ and $\mathcal{C}_{\text{forb}}$ respectively. An element $\mathbf{q} \in \mathcal{C}$ is called a *configuration point*, or *configuration* for short. Given a configuration $\mathbf{q} \in \mathcal{C}$ we denote by $A(\mathbf{q})$ the portion of the work space which is covered by A when it assumes the configuration $\mathbf{q}$ and it is called either *placement*, or *pose*, or simply *configuration*, when there is no risk of confusion. Similarly $R_0(\mathbf{q}), a_i(\mathbf{q}), E_i^A(\mathbf{q})$ and $\vec{n}_i^A(\mathbf{q})$ denote respectively the position, in the work space, of the reference point, i-th vertex, i-th edge or i-th normal of the robot.

For a configuration point $\mathbf{q} = (\vec{r}, \theta)$ we have

$$\begin{aligned} R_0(\mathbf{q}) &= \vec{r} + R_0 \\ E_i^A(\mathbf{q}) &= a_{i+1}(\mathbf{q}) - a_i(\mathbf{q}) \\ \vec{n}_i^A(\mathbf{q}) &= R^{\frac{\pi}{2}}\left(E_i^A(\mathbf{q})\right) \end{aligned}$$

where $\vec{r} = (x, y)$ is the translation component of the configuration, θ is the rotational component and R^α is the standard (counterclockwise) *rotation matrix* (cf. Figure 1). In order to express $a_i(\mathbf{q})$ for an arbitrary configuration $\mathbf{q}$ we have to choose a model of the configuration space. In this paper we consider two possible models

$$\mathcal{C}^{\text{geom}} = \left\{(x, y, \theta) \mid (x, y) \in \mathbb{R}^2, \theta \in [0, 2\pi)\right\} \tag{1}$$

$$\mathcal{C}^{\text{rat}} = \left\{(x, y, \tau) \mid (x, y) \in \mathbb{R}^2, \tau \in \mathbb{R} \cup \infty\right\} \tag{2}$$

which we call the *geometrical* and *rational* models respectively. When no confusion can arise, we shall simply write $\mathcal{C}$ to denote the configuration space. Note that $\mathcal{C}^{\text{geom}} = \mathbb{R}^2 \times S^1$ and $\mathcal{C}^{\text{rat}} = \mathbb{R}^2 \times \mathbb{RP}^1$. Finally, these models are related by $\tau = \tan\frac{\theta}{2}$.

For $\mathbf{q} = (\vec{r}, \theta) \in \mathcal{C}^{\text{geom}}$ we have

$$a_i(\mathbf{q}) = \vec{r} + R^\theta a_i(\mathbf{0}) = \vec{r} + R^\theta a_i. \tag{3}$$

On the other hand, given a configuration point $\mathbf{q}' = (\vec{r}, \tau) \in \mathcal{C}^{\text{rat}}$ with $\tau \in \mathbb{R} \cup \infty$ we have

$$a_i(\mathbf{q}') = \vec{r} + M^\tau a_i \tag{4}$$

where M^τ is the so called *rational rotation matrix* which is given by

$$M^\tau = \frac{1}{1+\tau^2} \begin{pmatrix} 1-\tau^2 & -2\tau \\ 2\tau & 1-\tau^2 \end{pmatrix}. \tag{5}$$

Note that since $\lim_{\tau \to \pm\infty} M^\tau = R^\pi$ we can safely set $M^\infty = R^\pi$.

Before we continue, we would like to note the following two remarks.

Remark 1. When using the rational representation of the configuration space and taking rational coordinates for the translation vector $\vec{r}$ and letting $\tau \in \mathbb{Q}$, it is possible to establish *exact rational* computations. On the other hand, the geometrical representation is of more use when one is trying to visualize elements of the configuration space. This is due to the fact that the rotation component in $\mathcal{C}^{\text{geom}}$ is bounded.

Remark 2 (The Group Structure). The configuration space in our case, namely the one which corresponds to a planar robot which is free to rotate and translate (this kind of robot is also called *holonomic*), is homeomorphic to the *special Euclidean group* $SE(2)$. Indeed, the following homeomorphisms hold

$$SE(2) \cong \mathbb{R}^2 \times S^1 \cong \mathbb{R}^2 \times \mathbb{RP}^1.$$

See [14, §4.2] for further details.

1.2 Contacts and the Boundary of the Forbidden Space

We say that $A(\mathbf{q})$ *touches* or is *in contact* with an obstacle O for a configuration $\mathbf{q}$ if

$$\partial A(\mathbf{q}) \cap \partial O \neq \emptyset \text{ and } \text{int}(A(\mathbf{q})) \cap \text{int} O = \emptyset.$$

Recall that $A(\mathbf{q})$ touches O if and only if $\mathbf{q} \in \partial \mathcal{C}_{\text{forb}}$ [14, §4.3]. If only

$$\partial A(\mathbf{q}) \cap \partial O \neq \emptyset,$$

then we say that $A(\mathbf{q})$ *pseudo touches* or is *in pseudo contact* with the obstacle O. In this case we clearly have that $\mathbf{q} \in \mathcal{C}_{\text{forb}}$.

For a configuration $\mathbf{q}$, such that the A pseudo touches *or* just touches an obstacle O, one or more of the following *contact types* can hold:

Name	Notation	Definition
Vertex-Edge	$(\text{v}_i\text{-e}_j)$	$a_i(\mathbf{q}) \cap \text{int} E_j^O \neq \emptyset$
Edge-Vertex	$(\text{e}_i\text{-v}_j)$	$\text{int} E_i^A(\mathbf{q}) \cap b_j \neq \emptyset$
Vertex-Vertex	$(\text{v}_i\text{-v}_j)$	$a_i(\mathbf{q}) = b_j$
Edge-Edge	$(\text{e}_i\text{-e}_j)$	$\lvert \text{int} E_j^A(\mathbf{q}) \cap \text{int} E_j^O \rvert > 1$

Note that the contact type alone does not imply whether the interiors of the robot and the obstacle intersect or not. Note, in addition, that a robot can maintain various (pseudo) contacts with the same obstacle simultaneously. In the presence of more then one obstacle then it can maintain multiple contacts as well. The following definitions refer to portions of $\mathcal{C}_{\text{forb}}$ which maintain a fixed (pseudo) contact with a given obstacle.

Definition 3 (Contact Surface)**.** The set of all configuration points which correspond to a *pseudo contact* between a vertex (or an edge) of the robot and a vertex (or an edge) of an obstacle is called a *contact surface*.

Note that a contact surface is a subset of $\mathcal{C}_{\text{forb}}$, since a configuration which realizes a pseudo contact can, in the same time, realize an intersection of the interiors of the robot and an obstacle. The following definition focuses on the configurations which realize *contacts*.

Definition 4 (Contact Patch)**.** The set of all configuration points which correspond to a *contact* between a vertex (or an edge) of the robot and a vertex (or an edge) of an obstacle is called a *contact patch*.

Every contact between a robot and an obstacle is also a pseudo contact, thus we have that each contact patch is a subset of a contact surface. Furthermore, it is a subset of $\partial\mathcal{C}_{\text{forb}}$. In addition, the union of all contact patches is the boundary of the forbidden space. Finally, a contact surface which maintains a (v-e) or (e-v) contact is of dimension two, whereas a contact surface which maintains either (v-v) contact or (e-e) contact is of dimension one. This means that the boundary $\partial\mathcal{C}_{\text{forb}}$ is a union of contact patches of dimension two which are "glued" together with contact patches of dimension one. In Figure 3 an example of a pose which maintains various contact types is illustrated. Finally, a single obstacle is represented as a pillar-like object which is depicted in Figure 12. The portion of $\mathcal{C}$ which is bounded inside this pillar-like is the forbidden space which corresponds to the obstacle which was considered. If the work space contains more then one obstacle, then each one of them contribute another pillar-like object in the configuration space. The union of the interiors of the pillars is the forbidden space which corresponds to the work space.

In this paper we will formulate an explicit parameterization of the contact surfaces depending on the properties of the robot and the obstacles. Furthermore, we will find a subset of the parameter domain, of each contact surface, which corresponds to the respective contact patch. Thus, we will be able to parameterize the whole boundary of the forbidden space.

2 Rotating the Robot

Since the robot A that we consider is holonomic, every point $P \in \mathcal{W}$ can be a center of rotation of the robot. In particular, given a configuration point $\mathbf{q} \in \mathcal{C}$, the robot can rotate about every boundary point $\partial A(\mathbf{q}) \in \mathcal{W}$. This kind of motion, which is illustrated in Figure 4, is the corner stone of the parameterization that we formalize in this paper.

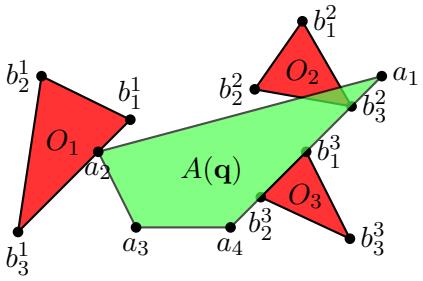

Figure 3: In this example, the configuration $\mathbf{q}$ corresponds to a (v_2-e_3) contact with O_1 and a (e_4-v_3) pseudo contact with O_2. In addition, with O_3 the robot maintains (v_4-e_2), (v_4-e_1) and (e_4-e_1) simultaneously. This means that $\mathbf{q}$ belongs both to four contact patches and to a contact surface.

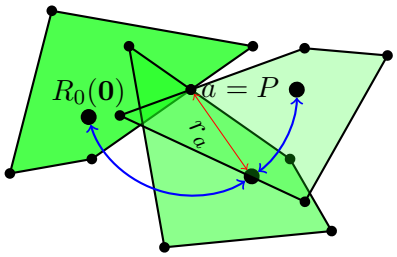

Figure 4: Rotating the robot about a fixed point on its boundary

Let us, for the time being, ignore all obstacles in the work space and assume that A can freely move in it. We set a point $P \in \mathcal{W}$ and mark a point $a \in \partial A(\mathbf{0})$ on the boundary of the robot when in the rest position. See the example in Figure 4. According to the notations standards that we use, $a(\mathbf{0}), a(\mathbf{q})$ denote the position of the marked point when the robot is in either the rest position or in some pose corresponding to a configuration $\mathbf{q}$. We will parameterize the set of configuration points in which the marked point a is fixed to the point P. More precisely, we want to parameterize the following set

$$P_a = \{\, \mathbf{q} \in \mathcal{C} : a(\mathbf{q}) = P \,\}\,. \tag{6}$$

Since the robot is rigid we have that the locus $\{R_0(\mathbf{q})\}_{\mathbf{q}\in P_a}$ is clearly a circle in the work space with center P and radius $r_a = \|R_0 - a\|$ (cf. Figure 4). For $\chi \in [0, 2\pi)$, this circle is parameterized by

$$P + r_a \begin{pmatrix} \cos\chi \\ \sin\chi \end{pmatrix} \tag{7}$$

Based on this intuition, we can prove the following lemma.

Lemma 5. *Given a point $P \in \mathcal{W}$ and a point $a \in \partial A$ the set P_a, as defined in Equa-*

tion (6), is parameterized by

$$\mathbf{q}_a(\phi) = \begin{pmatrix} \vec{r}_a(\phi) \\ \theta_a(\phi) \end{pmatrix} \tag{8}$$

where

$$\vec{r}_a(\phi) = P - R^\phi a \quad , \quad \theta_a(\phi) = \phi$$

for $\phi \in [0, 2\pi)$*. That is* $\mathbf{q} \in P_a$ *if and only if* $\mathbf{q} = \mathbf{q}_a(\phi)$ *for some* $\phi \in [0, 2\pi)$*.*

Proof. For some index i we have $a \in E_i^A$. Thus we can write $a = (1-t)a_i + ta_{i+1}$ for some $t \in [0, 1)$. First we show that if $\mathbf{q} = \mathbf{q}_a(\phi)$ for some ϕ then $\mathbf{q} \in P_a$, that is $a(\mathbf{q}) = P$. For every ϕ, using Equation (3), we have:

$$\begin{aligned} a_i(\mathbf{q}_a(\phi)) &= P - R^\phi a + R^\phi a_i \\ a_{i+1}(\mathbf{q}_a(\phi)) &= P - R^\phi a + R^\phi a_{i+1} \end{aligned}$$

In turn, we have

$$\begin{aligned} a(\mathbf{q}_a(\phi)) &= (1-t)a_i(\mathbf{q}_a(\phi)) + ta_{i+1}(\mathbf{q}_a(\phi)) \\ &= P - R^\phi a + (1-t)R^\phi a_i + tR^\phi a_{i+1} \\ &= P - R^\phi a + R^\phi((1-t)a_i + ta_{i+1}) \\ &= P - R^\phi a + R^\phi a = P \end{aligned}$$

This shows, that for every ϕ, the point $a(\mathbf{q}_a(\phi))$ is fixed to P.

Conversely, given $\mathbf{q} = (\vec{r}, \theta) \in P_a$ we have

$$P = a(\mathbf{q}) = \vec{r} + R^\theta a$$

Thus, $\vec{r} = P - R^\theta a$. Finally, for $\phi = \theta$ we have that $\mathbf{q} = \mathbf{q}_a(\phi)$. □

By mapping $\chi \mapsto \phi + \alpha_a + \pi$ in Equation (7) we can obtain the parameterization in Lemma 5. Using this re-parameterization we can observe that for $\phi = 0$ the parameterization given in Equation (8) is merely a translation. That is, the local frame which is assigned to the robot for $\mathbf{q}_a(0)$ is aligned with the global frame of the work space.

At this point it is important to point out that $\mathbf{q}_a(\phi)$ is meaningful only when interpreted as a point in $\mathcal{C}^{\text{geom}}$. We will see in details, in Section 4, a similar parameterization which is to be used when $\mathcal{C}^{\text{rat}}$ is the model of the configuration space. Finally, Equation (8) is a parameterization of a *helix* in the configuration space. We conclude this section with the following remark.

Remark 6 (Covering $\mathcal{C}$-Space with Helices). Instead of taking $a \in \partial A$, we can generalize the idea and consider an arbitrary linear combination of the vertices of the robot, $a = \sum_{i=1}^{n} \lambda_i a_i$, and some point $P \in \mathcal{W}$. The set of configurations which correspond to a rotation of the robot such that a is fixed to P is again a helix. As a matter of fact, every configuration point $\mathbf{q} \in \mathcal{C}$ is contained in infinitely many helices of this form.

3 Parameterizing Contact Surfaces

In this section we consider the robot A and *one convex* obstacle O. Later, an arbitrary obstacle can be decomposed into convex subsets and each sub-obstacle can be treated in a similar way. Given a (pseudo) contact type of A and O we will derive an explicit parameterization of the corresponding contact surfaces and patches.

3.1 Vertex-Edge Contact

A vertex-edge contact occurs when a vertex a_i of the robot lies in the interior of an edge E_j^O of the obstacle in a free manner, i.e. such that the interiors do not intersect (see O_1 and $A(\mathbf{q})$ in Figure 3 for an example). In this section, based on the parameterization obtained in Section 2, we will provide an explicit parameterization of the contact surface and the contact patch in the configuration space which correspond to the prescribed (v_i-e_j) pseudo contact and contact.

Let $P(t) = (1-t)b_j + tb_{j+1}$ be an arbitrary point in the interior of E_j^O. For $t \in (0,1)$ and $\phi \in [0, 2\pi)$ the configurations yielding the poses where a_i is fixed to $P(t)$ and rotating about it, are derived from Equation (8) by replacing P with $P(t)$ and setting $a = a_i$

$$\begin{aligned} S(t,\phi) =& \begin{pmatrix} P(t) - R^\phi a_i \\ \phi \end{pmatrix} \\ =& \begin{pmatrix} b_j - R^\phi a_i \\ \phi \end{pmatrix} + t \begin{pmatrix} b_{j+1} - b_j \\ 0 \end{pmatrix} \\ =& c(\phi) + t\vec{r}(\phi) \end{aligned} \tag{9}$$

Clearly, this surface is a *ruled surface* with directrix $c(\phi)$ and $\vec{r}(\phi) \neq 0$ as the vector field. Note that $\frac{d}{d\phi}\vec{r}(\phi) = 0$ which implies that S is a *cylindrical* ruled surface and thus *developable*. Note that for every $t' \in (0,1)$ we have that $S(t', \phi)$ is a helix. Furthermore, for $(0,1) \ni t'' \neq t'$ the helix $S(t'', \phi)$ is congruent to $S(t', \phi)$. Note that for $t \in \{0, 1\}$ the parameterization reduces to two helices which correspond to the two pseudo contacts (v_i-v_j) and (v_i-v_{j+1}) respectively (cf. Section 3.3). Clearly, as ϕ varies in the interval $[0, 2\pi)$, the configuration points on S represent both free *and* forbidden contact. In Figure 5, such a surface is illustrated.

Remark 7. If we fix a vertex a_i of the robot and generate all possible vertex-edge contact surfaces with all edges of the obstacle, then *helices* contained in each of these contact surfaces are congruent copies of each other. Note that if the obstacles are regular polygons then for a fixed vertex of the robot the contact surfaces are just congruent copies of each other. If, in addition, the robot is a regular polygon as well, then *all the vertex-edge contact surfaces* are congruent copies of each other.

Our next goal is to find a sub-domain $\Phi \subset [0, 2\pi)$ such that $S(t,\phi)_{|\phi\in\Phi}$ will be the *contact patch* which is contained in S. In Section 3.1.1 we analyze the domain $[0, 2\pi)$ of ϕ and find the sub-domain Φ. Appendix A.1 provide a similar analysis, using a different technique; this alternative approach has some limitations and advantages which are discussed.

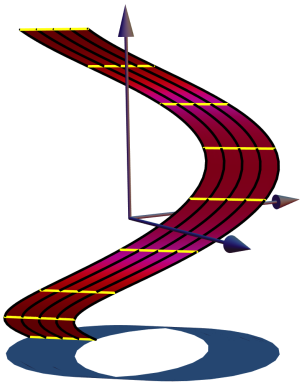

Figure 5: Example of a generic (v-e) contact *surface* in $\mathcal{C}$-space. The black curves are helices that correspond to $S(t_0, \phi)$ for $t_0 \in \{0, \frac{1}{4}, \frac{1}{2}, \frac{3}{4}, 1\}$. The yellow lines are the rulings of the surface.

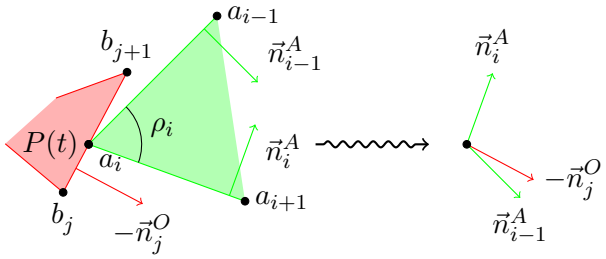

Figure 6: Generic setting of a (v-e) contact and the corresponding arrangement of the edge normals. Robot in green, and obstacle in red.

3.1.1 Vertex Edge Angle Range Analysis

By now, we given two indices i, j we derived the parameterization of the *contact surface* which corresponds to the (v_i-e_j) contact type. In particular, the configuration points on S correspond to all pseudo contacts between a_i and E^O_j. Let S be this surface, as given in Equation (9). Our next goal is to find a *contact patch* $S' \subset S \in \mathcal{C}$, such that for all $\mathbf{q} \in S'$ we will have that $a_i(\mathbf{q})$ *touches* the edge of the obstacle.

In particular, for each $t_0 \in (0, 1)$ we have to find a sub-domain $\Phi \subset [0, 2\pi)$ such that every point $\mathbf{q} \in S(t_0, \phi)\,|_{\phi \in \Phi}$ will yield a contact. Since we assume that both the robot and the obstacle are convex, the sub-domain Φ is independent of t_0. This can be seen in Figures 3 and 6. For some fixed $t_0 \in (0, 1)$ let $\mathbf{q}_i(\phi) = S(t_0, \phi)$ be a helix in S which correspond to the pseudo contact between the vertex a_i and the point $P = P(t_0)$ in the interior of the edge E^O_j. Note that $a_i(\mathbf{q}_i(\phi)) = P$ for all ϕ. Finally, the sub-domain Φ can be determined by finding two values:

- $\phi_{\min}$: The angle for which $a_{i+1}(\mathbf{q}_i(\phi_{\min}))$ lies on the line containing the edge E^O_j and $a_{i-1}(\mathbf{q}_i(\phi_{\min}))$ lies to the right of this edge.
- ϕ_{range}: The range of rotation which maintains the contact of a_i with the point P.

In practice this means that we want to have that $a_{i-1}((\mathbf{q}_i(\phi_{\min}+\phi_{\text{range}}))$ will lie on the line containing E_j^O such that $a_{i+1}(\mathbf{q}_i(\phi_{\min}+\phi_{\text{range}}))$ will lie to its right. See Figure 6 for an illustration of the setting we consider.

Let $\phi_{\max}=\phi_{\min}+\phi_{\text{range}}$ and define

$$\Phi=\begin{cases}[\phi_{\min},\phi_{\max}] & \text{if } \phi_{\max}<2\pi\\ [\phi_{\min},2\pi)\cup[0,\phi_{\max}-2\pi] & \text{if } \phi_{\max}\geq 2\pi\end{cases} \tag{10}$$

In turn, for all $\phi\in\Phi$ we have $a_i(\mathbf{q}_i(\phi))=P$. Conversely, if for some configuration $\mathbf{q}$ there is a *contact* between a_i and the point P on the edge E_j^O, then there exists some $\phi_0\in\Phi$ such that $\mathbf{q}=\mathbf{q}_i(\phi_0)$. Note that Φ as defined above is maximal only if P is an interior point of E_j^O. Otherwise, the sub-domain Φ is larger. This, however, is the case of vertex-vertex contact which we consider in Section 3.3.

We now compute the values of $\phi_{\min}$ and ϕ_{range}. The latter is straightforward to find, and depends on the interior angle at the vertex a_i of A, namely

$$\phi_{\text{range}}=\pi-\rho_i$$

Computing $\phi_{\min}$. We want to find ϕ such that for $\mathbf{q}_i(\phi)\in\mathcal{C}$ the following will hold:

$$P-\|E_i^A\|\frac{E_j^O}{\|E_j^O\|}=a_{i+1}(\mathbf{q}_i(\phi)),$$

where E_j^O is consider as the vector from b_j to b_{j+1} and $\|\cdot\|$ denotes the length of an edge. Solving this equation for ϕ is equivalent to solving

$$-\|E_i^A\|\frac{E_j^O}{\|E_j^O\|}=M\cdot(x,y)^T,$$

where $x=\cos\phi$, $y=\sin\phi$ and

$$M=\left(E_i^A,R^{\frac{\pi}{2}}\cdot E_i^A\right)^T. \tag{11}$$

Since $\det M=\|E_i^A\|^2\neq 0$, this system has a unique solution, denoted by $(x_0,y_0)^T$. We define $\{\phi_i\}_{i=1}^4$ as follows

$$\begin{aligned}\{\phi_1,\phi_2\}&=\arccos(x_0)\cap[0,2\pi)\\ \{\phi_3,\phi_4\}&=\arcsin(y_0)\cap[0,2\pi)\end{aligned}$$

Note that since (x_0,y_0) is a unit vector, we have that $\{\phi_1,\phi_2\}\cap\{\phi_3,\phi_4\}$ contains exactly one element. As $\phi_{\min}$ should lie in $[0,2\pi)$, it satisfies

$$\phi_{\min}=\{\phi_1,\phi_2\}\cap\{\phi_3,\phi_4\}.$$

For any combination of signs of x_0 and y_0 Table 1 suggests in which interval $\phi_{\min}$ is, and using the definition of the ϕ_i's it can be easily found. Finally, the red patches in Figure 12 correspond to all possible vertex-vertex contacts between triangular robot and obstacle.

x_0	y_0	$\phi_{\min} \in$
≥ 0	≥ 0	$[0, \frac{\pi}{2}]$
< 0	≥ 0	$[\frac{\pi}{2}, \pi]$
< 0	< 0	$[\pi, \frac{3\pi}{2}]$
≥ 0	< 0	$[\frac{3\pi}{2}, 2\pi]$

Table 1: The interval containing $\phi_{\min}$, depending on signs of x_0 and y_0 for the vertex-edge and edge-vertex contact types.

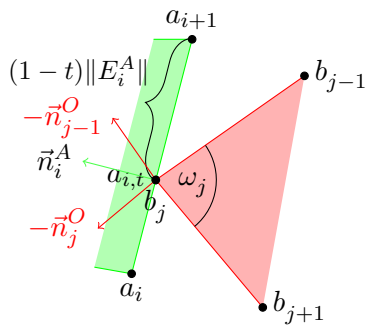

Figure 7: Generic setting of an (e-v) contact and the corresponding arrangement of the edge normals.

3.1.2 On the Exactness

The steps that we described so far, in general, cannot yield exact value of $\phi_{\min}$ since one has to compute the inverses of both the sine and cosine functions. Furthermore, the matrix M in Equation (11) involves the trigonometric functions as well, and thus cannot be represented in an exact manner. In turn, this means that x_0 and y_0 above cannot be computed exactly in the first place. In Appendix A.1 we find the sub-domain Φ without using trigonometrical functions, and thus it is represented exactly. In order to exploit this advantage, one has to impose the restriction that the vertices of the robot all lie on a circle of some fixed radius. This, however, is a very restrictive assumption. Finally, since we consider $\mathcal{C}^{\text{geom}}$ as the model of the configuration space, the parameterization of the contact surface (patch) itself, given in Equation (9), involves the trigonometric functions and in turn it could not be computed in an exact manner.

3.2 Edge-Vertex Contact

Recall that Equation (8) parameterizes a rotation of the robot about a point P such that a boundary point $a \in \partial A$ is fixed to P. For any $t \in (0, 1)$ we denote

$$a_{i,t} = (1-t)a_i + ta_{i+1} \tag{12}$$

to be the point on the edge E_i^A of the robot which is to be in pseudo contact with b_j. Next, in Equation (8), we replace P with b_j and a with $a_{i,t}$ and obtain

$$\begin{aligned} S(t,\phi) &= \begin{pmatrix} b_j - R^\phi a_{i,t} \\ \phi \end{pmatrix} \\ &= \begin{pmatrix} b_j - R^\phi a_i \\ \phi \end{pmatrix} + t \begin{pmatrix} -R^\phi \cdot E_i^A \\ 0 \end{pmatrix} \\ &= c(\phi) + t\vec{r}(\phi). \end{aligned} \tag{13}$$

for $t \in (0,1)$ and $\phi \in [0, 2\pi)$. $S(t,\phi)$ is the contact surface corresponding to the (e_i-v_j) pseudo contact. Again, like the parameterization in Equation (9) we obtain a ruled surface. We will study its geometry further in Sections 6.1 and 6.1. We stress that configuration points on this surface lie both in $\partial\mathcal{C}_{\text{forb}}$ and in the interior of $\mathcal{C}_{\text{forb}}$, since this is a contact *surface*.

In order to find the contact *patch* which is contained in S, as before, we have to find a sub-domain $\Phi \subset [0, 2\pi)$ for which $S(t,\phi)_{|\phi\in\Phi}$ is a collection of configuration points which corresponds to contacts and *not* to pseudo contacts. Again, as can be seen in Figure 7, the sub-domain Φ does not depend on t. Like before, we will provide two methods; one in Section 3.2.1 which is less restrictive but involves computations of trigonometric functions and thus inexact. The other, in Appendix A.2, is more accurate but at the same time more restrictive.

Remark 8. In contrast to the case of (v-e) (pseudo) contacts, here in the edge-vertex case we have that each contact surfaces is a collection of helices which are *not* congruent since their radii depend on $a_{i,t}$. This suggests, as we establish in Sections 6.1 and 6.1, the (e-v) contact surfaces are *not developable*.

3.2.1 Edge-Vertex Angle Range Analysis

In this section, we will find, like we did in Section 3.1.1, a sub-domain $\Phi \subset [0, 2\pi)$ such that $S(t,\phi)_{|\phi\in\Phi}$ is the *contact patch* which is contained in the contact surface S. To that end, we shall compute $\phi_{\min}, \phi_{\text{range}}$ and $\phi_{\max} = \phi_{\min} + \phi_{\text{range}}$ and we will set Φ as defined in Equation (10). As $\phi_{\min}$ and ϕ_{range} depend only on the indices i and j but not on t, we shall fix some $t_0 \in (0,1)$ and let $\mathbf{q}_i(\phi) = S(t_0,\phi)$. In this case, we have that $a_{i+1}(\mathbf{q}_i(\phi_{\min}))$ has to lie on the line containing E_{j-1}^O, such that the interiors of the robot and the obstacle do not intersect. Similarly, $a_i(\mathbf{q}_i(\phi_{\max}))$ has to lie on the line segment containing E_j^O (cf. Figure 7). Clearly, we have that

$$\phi_{\text{range}} = \pi - \omega_j.$$

It is left to find the value of $\phi_{\min}$.

Computing $\phi_{\min}$. In the case of (e-v) contact, the minimal angle of rotation $\phi_{\min}$ is the one for which the following will hold

$$\left.\begin{aligned} a_{i+1}(\mathbf{q}_i(\phi)) - b_j \parallel b_j - b_{j-1} \\ a_{i,t_0}(\mathbf{q}_i(\phi)) = b_j \end{aligned}\right\} \tag{14}$$

See Figure 7 for reference. First note that

$$\forall \mathbf{q} \in \mathcal{C} \quad \|a_{i+1}(\mathbf{q}) - a_{i,t}(\mathbf{q})\| = (1-t)\,\|E_i^A\|.$$

Thus, in order to find ϕ such that the conditions in (14) will hold we have to solve the following equation

$$b_j - (1-t_0)\,\|E_i^A\|\,\frac{E_{j-1}^O}{\|E_{j-1}^O\|} = a_{i+1}(\mathbf{q}_i(\phi)),$$

with ϕ as the unknown. Like in the previous computation of $\phi_{\min}$, the last equation can be rewritten as

$$(t_0-1)\|E_i^A\|\frac{E_{j-1}^O}{\|E_{j-1}^O\|} = M \cdot (x,y)^T$$

with $x = \cos\phi$, $y = \sin\phi$ and

$$M = \left(a_{i+1} - a_{i,t_0}, R^{\frac{\pi}{2}} \cdot (a_{i+1} - a_{i,t_0})\right)^T, \tag{15}$$

similarly to the matrix in Equation (11). Since $\det M = (1-t_0)^2\,\|E_i^A\|^2 \neq 0$, the system above has a unique solution, namely

$$(x_0, y_0)^T = (t_0-1)\frac{\|E_i^A\|}{\|E_{j-1}^O\|} M^{-1} \cdot E_{j-1}^O.$$

Note that since the matrix in Equation (15) contains trigonometric function and the solutions x_0, y_0 are obtained using inverse trigonometric functions, the values that we compute for $\phi_{\min}$ using this method cannot be represented exactly. In Appendix A.2 we present a method, analogous to the one showed in Appendix A.1, which can yield exact representation of Φ. In any case, as we discussed in Section 3.1.2, the end, due to the model of $\mathcal{C}$ in use, namely $\mathcal{C}^{\text{geom}}$, and the nature of the corresponding parameterization itself, which involves trigonometric function, the contact patches itself cannot be exactly represented. Finally, we refer to Figure 12, where the green patches correspond to the edge-vertex contacts.

3.2.2 Generalizing the Edge

In Section 3.2 we derived a parameterization of an (e-v) contact surface. We can assume, with out loss of generality, that the edge E_i^A, when in the rest position, is horizontal and at distance d from the origin. Let ℓ be the line which contains the edge. Furthermore, let $a_t = (t, d)$ be a varying point on the line ℓ. This generalizes the case, and shows that the properties of the contact surface depend on the distance of the edge of the robot from the origin. See an illustration in Figure 8. By replacing a with a_t and setting $P = (0,0)$ we obtain from Equation (8) the following parameterization in $\mathcal{C}$

$$S(t,\phi) = \begin{pmatrix} -R^{\phi} a_t \\ \phi \end{pmatrix} \tag{16}$$

with $\phi \in [0, 2\pi)$ and $t \in \mathbb{R}$. In Figure 9 an example of such generalized edge-vertex contact surface is plotted.

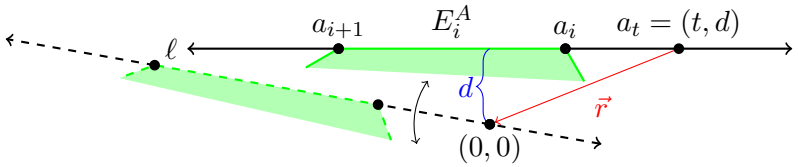

Figure 8: An infinite edge with a vertex a_t on it in solid and its translated and rotated pose where a_t coincides with the origin.

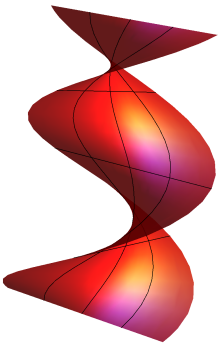

Figure 9: An example of a general edge-vertex contact surface for $d = 0.5$.

3.3 Vertex-Vertex and Edge-Edge Contacts

Motions of the robot that maintain either a vertex-edge or an edge-vertex contact have two degrees of freedom. In the previous sections we parameterized these motions, and, indeed, the developed parameterization yielded contact surfaces (and patches) of dimension two. In order to complete the picture we have to consider the configurations that correspond to vertex-vertex and edge-edge (pseudo) contacts. Motions maintaining these contacts have only *one* degree of freedom. We recall that the boundaries of the two dimensional contact patches that we derived are exactly the one dimensional contact patches. Indeed, we will use the parameterization that we obtained and express explicitly the parameterizations of the vertex-vertex and edge-edge contacts.

3.3.1 Vertex-Vertex Contact

For two indices i and j, the corresponding (v_i-v_j) pseudo contact is parameterized by

$$C(\phi) = S(0, \phi)$$

for $\phi \in [0, 2\pi)$ and $S(\cdot, \cdot)$ as given in Equation (9). Note that for $\phi \in [0, 2\pi)$ we obtain a contact *surface* (actually a single helix), since it corresponds to (v_i-v_J) pseudo contacts that are not contacts. In order to find the interval Φ which correspond to the (v-v) *contacts* alone, we compute $\phi_{\min}$ that corresponds to the (v_i-e_{j-1}) contact. For the pose which corresponds to $C(\phi_{\min})$ we have that a_i coincides with b_j, a_{i+1} lies on the line

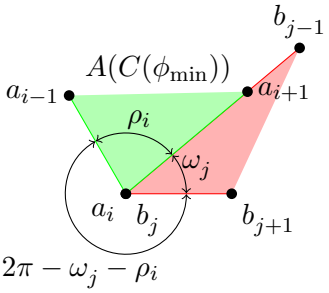

Figure 10: Illustration of a vertex-vertex contact with $C(\cdot)$ and $\phi_{\min}$ as defined in Section 3.3.1.

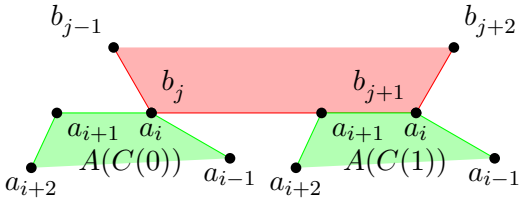

Figure 11: Setting of an edge-edge contact where $C(\cdot)$ is given in Section 3.3.2.

containing E^O_{j-1} and a_{i-1} lies to the right of this edge. See Figure 10 for an illustration. For Φ as defined in Equation (10) with $\phi_{\max} = \phi_{\min} + 2\pi - \omega_j - \rho_i$ we get the sub-helical-arc $C(\phi)_{|\phi\in\Phi}$ that corresponds to the (v-v) contacts alone.

3.3.2 Edge-Edge Contact

Parameterizing the configurations which correspond to an (e_i-e_j) contact can be again obtained using the parameterization of the corresponding (v_i-e_j) contact. Let us set

$$C(t) = S(t, \phi_{\min})$$

where $S(\cdot,\cdot)$ is given in Equation (9) and $\phi_{\min}$ is the one defined in Section 3.1.1. In this case we have that $C(0)$ corresponds to a (v_i-v_j) contact and $C(1)$ corresponds to a (v_i-v_{j+1}) contact. In both cases a_{i+1} lies on the line containing E^O_j. Figure 11 illustrates the situation and, in addition, suggests that for $t \in [0,1)$ we do not obtain the whole (e_i-e_j) contact. In order to complete the case, we have to let $t \in \left(0, 1 + \frac{\|E^A_i\|}{\|E^O_j\|}\right)$.

3.4 Conclusion

In this section we derived, based on the fundamental motion described in Section 2, the parameterization of all the elements of the boundary of the forbidden space which correspond to a single obstacle. Each obstacle in the work space contributes a pillar-like

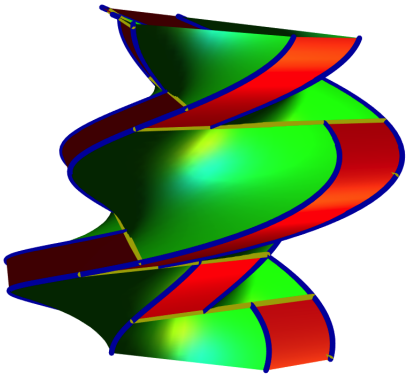

Figure 12: An example of all possible contact patches for a given robot and one obstacle in $\mathcal{C}$. In red and green are the (v-e) and (e-v) contact patches respectively. The blue helical arcs correspond to (v-v) contacts and the yellow (straight) line segments correspond to (e-e) contacts.

object, similar to the one depicted in Figure 12. Given an obstacle O, the portion of $\mathcal{C}$ which is bounded "inside" the corresponding pillar-like object is the forbidden space related to O. The portion of the configuration space which is bounded inside all the pillars, is the forbidden space.

We will conclude the section by noting that most of the patches that we visualize in Figure 12 are bounded from all sides by contact patches of dimension one. However, some of them do not; this is due to the fact that we visualize $\mathcal{C}^{\text{geom}} \cong \mathbb{R}^2 \times S^1$. Cases where we had to split Φ into two connected components correspond to contact patches that are visualized as disconnected. This is obviously merely an artifact of the visualization, as we have to restrict ourselves to an Euclidean space.

4 Rational Parameterization

So far, in our discussion, we considered $\mathcal{C}^{\text{geom}}$ as the model of the configuration space. In other words, we used $\mathbb{R}^2 \times S^1$ to model the configuration space $\mathcal{C}$, such that the first two coordinates correspond to the translation component of the configuration points and the third coordinate corresponds to the *angle* of a rotation. This representation, of the configuration space, provides a strong and direct geometrical intuition which can be utilized to visualization purposes as we saw, for example, in Section 3. However, this representation introduces one prominent drawback. Namely, even if the coordinates of the vertices of the robot can be represented exactly (see Section 1.1), the contact surfaces that we derive *cannot* be represented exactly as their parameterization, cf. Equations (8), (9) and (13), involves trigonometric functions. This fact means, for example, that intersecting a contact patch with a line segment in the configuration space cannot yield *exact* results when the geometrical model $\mathcal{C}^{\text{geom}}$ is in use.

By switching to $\mathcal{C}^{\text{rat}}$ as the model of the configuration space, we can overcome this problem, and obtain a rational-based parameterization of the contact surfaces and

patches. In other words, we can parameterize the contact surfaces using rational functions. Recall that given a configuration point $\mathbf{q} = (\vec{r}, \theta) \in \mathcal{C}^{\text{geom}}$ with $\theta \in [0, 2\pi)$ we have that

$$\begin{aligned} a_i(\mathbf{q}) &= \vec{r} + R^\theta a_i \\ &= \vec{r} + M^\tau a_i = a_i(\mathbf{q}') \end{aligned}$$

where $\mathbf{q}' = (\vec{r}, \tau) \in \mathcal{C}^{\text{rat}}$, M^τ is the rational rotation matrix and

$$(-\infty, \infty] \ni \tau = \tau(\theta) = \begin{cases} \tan\frac{\theta}{2} & \text{if } \theta \neq \pi \\ \infty & \text{otherwise} \end{cases} \tag{17}$$

Similarly to the study in the case where we used $\mathcal{C}^{\text{geom}}$, we obtain a parameterization in $\mathcal{C}^{\text{rat}}$ of a rotation of the robot A such that $a \in \partial A$ is fixed to a point P in the work space which is given by

$$\mathbf{k}_a(\psi) = (\vec{r}_a(\psi), \tau_a(\psi)) \tag{18}$$

with $\vec{r}_a(\psi) = P - M^\psi a$ and $\tau_a(\psi) = \psi$. Finally, by either letting $P = P(t) = (1-t)b_j + tb_{j+1}$ vary along an edge of the obstacle or letting $a = a_{i,t} = (1-t)a_i + ta_{i+1}$ vary along an edge of the robot, we obtain two *rational* parameterizations

$$S(t, \psi) = \begin{pmatrix} P(t) - M^\psi a_i \\ \psi \end{pmatrix} \tag{19}$$

$$S(t, \psi) = \begin{pmatrix} b_j - M^\psi a_{i,t} \\ \psi \end{pmatrix} \tag{20}$$

with $\psi \in (-\infty, \infty]$ and $t \in (0, 1)$ of the (v_i-e_j) and (e_i-v_j) contact *surfaces* respectively.

Next, we want to find a sub-domain $\Psi \subset (-\infty, \infty]$ which will correspond to the contact patches in the configuration space. Given a two dimensional contact type let $\phi_{\min}$ and $\phi_{\max}$ be the values that we compute in Sections 3.1.1 and 3.2.1. Using Equation (17) we can find the corresponding $\psi_{\min}$ and $\psi_{\max}$. In turn, Ψ can be defined as follows:

$$\Psi = \begin{cases} [\psi_{\min}, \psi_{\max}] & \text{if } 0 \leq \phi_{\min}, \phi_{\max} \leq \pi \vee \pi < \phi_{\min}, \phi_{\max} < 3\pi \\ [\psi_{\min}, \infty] \cup (-\infty, \psi_{\max}] & \text{if } \phi_{\min} \in [0, \pi] \wedge \phi_{\max} \in (\pi, 2\pi) \end{cases}$$

Finally, the missing one dimensional contact patches can be easily obtained by considering the boundaries of the contact patches which were derived.

5 Normals of the Contact Patches

For a single obstacle O, the union of the corresponding contact patches constitute the boundary between the free and forbidden space. In other wards, for a configuration point $\mathbf{q} \in S$, for some contact patch S, we have that $A(\mathbf{q})$ touches the obstacle O. In particular, for some ε we have that the configuration point $\mathbf{q} + \varepsilon\mathcal{N}_S(\mathbf{q})$ corresponds to either a collision between A and O or a free placement of A with respect to O. Here

$\mathcal{N}_S(\mathbf{q})$ denotes the *normal* to the surface S at the point $\mathbf{q} \in S$. Recall, that for a surface $S(t,\phi)$, its unit normal is given by $\frac{\partial_t S \times \partial_\phi S}{\|\partial_t S \times \partial_\phi S\|}$, where $\partial_t S$ and $\partial_\phi S$ are the partial derivatives of S. We however, for the sake of simplicity of the expressions, consider here

$$\mathcal{N}_S(t,\phi) = \partial_t S \times \partial_\phi S$$

without normalization. In this section we will study the surface normals of the contact patches that we derived in the previous sections. This information can be helpful when one studies the configuration space and address the motion planning problem (cf. [25, 24]).

The following two lemmas can be directly proved.

Lemma 9 (Vertex-edge case)**.** *If $S(t,\phi)$ is a vertex-edge contact patch, then we have*

$$\mathcal{N}_S(t,\phi) = -\begin{pmatrix} \vec{n}_j^O \\ \left\langle E_j^O, R^\phi a_i \right\rangle \end{pmatrix}$$

Lemma 10 (Edge-vertex case)**.** *If $S(t,\phi)$ is a edge-vertex contact patch, then we have*

$$\mathcal{N}_S(t,\phi) = \begin{pmatrix} R^{\frac{\pi}{2}+\phi}(a_{i+1} - a_i) \\ \langle a_{i,t}, a_{i+1} - a_i \rangle \end{pmatrix} = \begin{pmatrix} R^\phi \vec{n}_i^A \\ \langle a_{i,t}, E_i^A \rangle \end{pmatrix}$$

Note that in both cases the normals point towards the free portion of the configuration space. More precisely, if the work space contains only one obstacle, then the configuration point

$$S(t,\phi) + \varepsilon \mathcal{N}_S(t,\phi),$$

for some $\varepsilon > 0$, is in $\mathcal{C}_{\text{free}}$.

6 Differential Geometry of Contact Surfaces

Once one obtain the parameterization of the contact surfaces and patches it is natural and interesting to study their geometrical properties. Better understanding of these properties can be of help in the future to study further the configuration space in general and in the context of the motion planning problem. For example, establishing a discretization of the contact surfaces and patches can prove to be useful. We first, in Section 6.1, consider the surfaces and patches embedded in $\mathcal{C}^{\text{geom}}$ and later, in Section 6.2, we study the geometry of the boundary of the forbidden space when it is embedded in $\mathcal{C}^{\text{rat}}$.

6.1 Geometrical Model

As we saw in Section 3.1, the contact surfaces which correspond to (v-e) contacts are rather simple, namely *developable* surfaces. Therefore their geometry is rather simple as well – we thus leave their study to Appendix B.

In the remaining of this section we will study the geometrical properties of the (e_i-v_j) contact surfaces. For the sake of simplicity we assume that $P = b_j$ is at the origin. As

before, let us assume that $R_0(\mathbf{0})$ is at the origin as well. For $t \in (0,1)$ and $\phi \in [0, 2\pi)$ and using Equation (13) we have that the contact surface is given by

$$\begin{aligned} S(t,\phi) &= \begin{pmatrix} -R^\phi a_{i,t} \\ \phi \end{pmatrix} \\ &= \begin{pmatrix} -R^\phi a_i \\ \phi \end{pmatrix} + t \begin{pmatrix} -R^\phi \cdot E_i^A \\ 0 \end{pmatrix} \\ &= c(\phi) + t\vec{r}(\phi) \end{aligned}$$

where $a_{i,t} = (1-t)a_i + ta_{i+1}$ as before. Note that $\vec{r}(\phi), \frac{d}{d\phi}\vec{r}(\phi) \neq 0$; this means that the ($\mathrm{e}_i$-$\mathrm{v}_j$) contact surface is a *non-cylindrical ruled surface* [5, p. 190].

We start our study of the geometrical properties of the contact surface by computing its first (denoted E, F, G) and second (denoted e, f, g) fundamental forms.

$$\begin{aligned} E &= \|a_i - a_{i+1}\|^2 & e &= 0 \\ F &= \det(a_i, a_{i+1}) & f &= -\frac{\|a_i - a_{i+1}\|^2}{\nu} \\ G &= 1 + \|a_{i,t}\|^2 & g &= -\frac{\det(a_i, a_{i+1})}{\nu} \end{aligned}$$

where $\nu = \nu(t) = \sqrt{EG - F^2}$. It is easy to verify that $\nu \neq 0$ for all $t \in \mathbb{R}$, and thus, all expressions are well defined.

Gaussian and mean curvatures. Next, we can easily express the *Gaussian curvature*

$$\begin{aligned} K(t) = K(t,\phi) =& \frac{eg - f^2}{EG - F^2} \\ =& -\frac{\|a_i - a_{i+1}\|^4}{\nu^4} = -\frac{E^2}{\nu^4} \end{aligned} \tag{21}$$

Note that the Gaussian curvature depends *only* on t as ν depends on t, that is the point of contact along E_i^A. Similarly, the *mean curvature* is given by

$$\begin{aligned} H(t) = H(t,\phi) =& \frac{eG - 2fF + gE}{2(EG - F^2)} \\ =& \frac{\|a_i - a_{i+1}\|^2 \det(a_i, a_{i+1})}{2\nu^3} = \frac{EF}{2\nu^3} \end{aligned} \tag{22}$$

We see again that the mean curvature only depends on t. Furthermore, if the two vertices, a_i and a_{i+1}, considered as vectors with bases at the origin, are linearly dependent, then the mean curvature vanishes; thus the surface is a *minimal surface*. This yield the following lemma.

Lemma 11. *If the line through $E_i^A(\mathbf{0})$ contains the reference point $R_0(\mathbf{0})$, then the corresponding (e_i-v_j) contact surface is a* minimal surface *and thus a* helicoid.

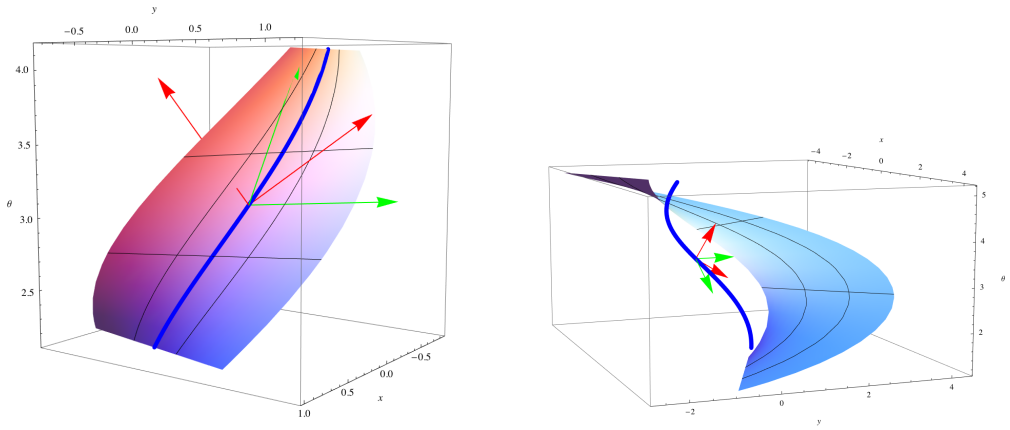

(a) Striction curve is on the patch.

(b) Striction curve is off the patch.

Figure 13: Two examples of an (e-v) contact surface. The green arrows are the *asymptotic directions* and the red ones are the *principal curvature directions*. In solid blue is the striction curve.

Extrema of curvatures and the striction curve. Both $\frac{d}{dt}K$ and $\frac{d}{dt}H$ vanish for the same single value of t, as can be easily verified, and it is given by

$$t_\star = \frac{\langle a_i, a_i - a_{i+1}\rangle}{E}.$$

We recall that the *striction curve* can be characterized as the locus of points where the Gaussian curvature attains and extremum [18]. Since $\lim_{t\to\pm\infty} K(t) = 0$ and $K(t) \neq 0$ for all t, we have that $K(t_\star)$ is a global extremum of the Gaussian curvature. Thus we have that the curve $S(t_\star, \phi)$ is the *striction curve* of the contact surface. The striction curve can also be computed directly, following, for example, the definitions given in [5]. Next, we can state the following theorem.

Theorem 12. *For any edge-vertex contact surface the extremum of the Gaussian curvature is*

$$\sup_{t\in\mathbb{R}} K(t) = -1$$

and independent of the properties of the robot.

Proof. Since $\sup_{t\in\mathbb{R}} K(t) = K(t_\star)$, it is enough to compute $K(t_\star)$. □

It is easy to verify that the point $a_{t_\star} = (1 - t_\star)a_i + t_\star a_{i+1} \in \ell$ is the closest point to the origin among all the points on the line ℓ which contains E_i^A. Thus, it is easy to see that $t_\star$ may not lie in the interval $[0, 1]$. That is, the striction curve of the (e-v) contact surface is not necessarily contained in the surface itself. See for example Figures 13a and 13b.

We conclude this paragraph, with the following observation. In contrast to the Gaussian curvature, the extremum of the mean curvature depends on the properties of the

robot. In particular, we have the following

$$\sup_{t\in\mathbb{R}} H(t) = H(t_\star) = \frac{d}{2},$$

where d is the distance of ℓ from the origin and is given by

$$d = \frac{\det(a_i, a_{i+1})}{\|a_{i+1} - a_i\|} = \frac{F}{\sqrt{E}}.$$

The normal curvature and friends. Next, we will compute the *normal curvature* of the surface, denoted by κ_N. In general, for a given unit tangent vector $\varepsilon \in T_{\mathbf{q}}S$, the normal curvature in its direction is given by $\kappa_N(\varepsilon) = II(\varepsilon, \varepsilon)$, where $II(\cdot, \cdot)$ denotes the *second fundamental form*. The first step we take is to set an orthonormal coordinate system in the tangent space $T_{\mathbf{q}}S$. Let

$$\begin{aligned} E_1 &= \frac{1}{\sqrt{E}}\frac{\partial S}{\partial t} \\ E_2 &= \frac{1}{\sqrt{E(EG - F^2)}}\left(E\frac{\partial S}{\partial \phi} - F\frac{\partial S}{\partial t}\right) \end{aligned} \tag{23}$$

be an orthonormal frame in $T_{\mathbf{q}}S$. Next, for each point $\mathbf{q} \in S$ and given some angle ξ we obtain a unit tangent vector

$$\varepsilon(\xi) = \cos\xi E_1 + \sin\xi E_2$$

in $T_{\mathbf{q}}S$. For the sake of completeness, let us note that $\varepsilon(\xi)$ can be expressed in terms of the standard coordinate system $\{\frac{\partial S}{\partial t}, \frac{\partial S}{\partial \phi}\}$ as:

$$\varepsilon(\xi) = \left(\frac{\sqrt{EG - F^2}\cos\xi - F\sin\xi}{\sqrt{EG - F^2}\sqrt{E}}\right)\frac{\partial S}{\partial t} + \frac{\sqrt{E}\sin\xi}{\sqrt{EG - F^2}}\frac{\partial S}{\partial \phi}.$$

Therefore, the normal curvature at $\mathbf{q} \in S(t, \phi)$ in direction ξ, with respect to the orthonormal coordinate system of the tangent plane $T_p(S)$, is given by [7]

$$\kappa_N(\xi) = \frac{E\sin\xi(F\sin\xi - 2\nu\cos\xi)}{\nu^3}. \tag{24}$$

Recall that ν depends on t and does not vanish for all $t \in \mathbb{R}$, and therefore Equation (24) is well defined. It is easy to note that the normal curvature depends only on the direction in the tangent plane, given by ξ, and the position on the ruling given by t.

Singularities and Extrema of the Normal Curvature. Next, we want to find the *asymptotic directions* and the *principal curvature directions* of the contact surface. In other words we want to find the values of ξ for which the normal curvature either vanishes or attains an extremum. Furthermore, we will find the extrema values of the normal curvature, that is, expressions of the *principal curvatures*.

As the rulings on the surface are straight lines, the normal curvature in their directions should vanish, and indeed for $\xi \in \{0, \pi\}$ the normal curvature vanishes. The other direction where it vanishes corresponds to

$$\xi = \arctan \frac{2\nu}{\det(a_i, a_{i+1})} = \arctan \frac{2\nu}{F} \tag{25}$$

The green arrows in Figure 13 point in the directions where the normal curvature vanishes. Note, that one of the arrows in each figure is parallel to the ruling's direction.

Remark 13. Note that if S is a minimal surface (and thus also a helicoid), then the denominator in Equation (25) vanishes. Thus, we have that the second direction for which the normal curvature vanishes corresponds to $\xi = \pi/2$. This coincide with the fact that for the helicoid the asymptotic directions are orthogonal [10].

We now want to find the principal curvature directions and to that end we have to derivative $\kappa_N(\xi)$ with respect to ξ. This yields

$$\frac{\partial}{\partial \xi}\kappa_N(\xi) = \frac{2E}{\nu^3}(F \sin\xi \cos\xi - \nu \cos 2\xi).$$

In turn, it can be verified that that for

$$\xi_1 = \frac{1}{2} \arctan \frac{2\nu}{F}$$

the normal curvature attains an extremum. Since the principal curvature directions are orthogonal, we have that it attains its other extremum for $\xi_2 = \xi_1 + \frac{\pi}{2}$. In Figure 13 the red arrows point in the principal curvature directions. Finally, the principal curvatures are

$$\kappa_1 = \kappa_N(\xi_1) \quad , \quad \kappa_2 = \kappa_N(\xi_2) \tag{26}$$

We can also express the principal curvatures explicitly

$$\kappa_1 = -\frac{2E}{\nu\left(F + \sqrt{F^2 + 4\nu^2}\right)}$$
$$\kappa_2 = \frac{E(F + \sqrt{F^2 + 4\nu^2})}{2\nu^3}.$$

Note that indeed $K = \kappa_1\kappa_2$ as in Equation (21) and $H = \frac{\kappa_1+\kappa_2}{2}$ as in Equation (22).

Remark 14. The principal curvatures could have been computed directly using formulas which base on the fundamental forms. We took a longer path as we wanted to obtain expressions for the principal curvature directions as well.

Generalized edge-vertex case. We shall conclude this section with the study of the geometry of the general contact surface which we introduced in Section 3.2.2. In particular, we derive expressions of the Gaussian, mean and normal curvatures, as well as the principal curvatures directions and their magnitudes. For a *fixed* distance d we have the following expressions

$$K = -\frac{1}{(1+t^2)^2}$$
$$H = -\frac{d}{2\sqrt{(1+t^2)^3}},$$

for the Gaussian and mean curvatures respectively. As before, the normal curvature in the direction of a unit tangent vector $\varepsilon(\xi)$ is

$$\kappa_N = -\frac{\sin\xi(2\sqrt{1+t^2}\cos\xi + d\sin\xi)}{\sqrt{(1+t^2)^3}}$$

where ξ parameterizes the direction in the tangent space of the unit vector $\varepsilon(\xi)$. It comes as no surprise that all the curvatures depends only on t. In terms of the motion of the robot, it means that the curvatures of an (e-v) contact surface depends only on the position of a_t on the line ℓ, and *not* on the angle at which it touches the origin (that is the dummy vertex of an obstacle). Furthermore, the Gaussian curvature does not even depend on the distance of the edge from the origin; i.e. it does not depend on the properties of the robot. Note that for $d = 0$ the mean curvature vanishes; that is, the corresponding surface is a minimal one. Recall that $d = 0$ means that the general edge is passing through the origin and this coincides with the result of Lemma 11.

We have that the normal curvature vanishes for

$$\xi_0 = 0 \quad , \quad \xi_1 = \arctan\left(-\frac{2\sqrt{1+t^2}}{d}\right).$$

and its derivative with respect to ξ vanishes for

$$\xi_2 = \frac{1}{2}\xi_1 \quad , \quad \xi_3 = \frac{1}{2}\xi_1 + \frac{\pi}{2}.$$

Therefore at the point $S(t,\phi) \in S$, the vectors $\varepsilon(\xi_0)$ and $\varepsilon(\xi_1)$ point in the asymptotic directions and $\varepsilon(\xi_2)$, $\varepsilon(\xi_3)$ point in the principal curvature directions. Finally, the principal curvatures are

$$\kappa_1 = \kappa_N(\xi_2) = \frac{-d + \sqrt{4 + d^2 + 4t^2}}{2\,(1+t^2)^{3/2}}$$
$$\kappa_2 = \kappa_N(\xi_3) = \frac{d + \sqrt{4 + d^2 + 4t^2}}{2\,(1+t^2)^{3/2}}$$

Let us conclude by pointing out that both the Gaussian and the mean curvatures attain their extrema for $t = 0$. For the Gaussian curvature we have that its extremum

is -1 and the extremum of the mean curvature is $\frac{d}{2}$. The striction curve of the general edge-vertex contact surface is attained when fixing $t = 0$ where the point a_t with $t = 0$ is the closest point of the line ℓ to the origin. All these results coincide with previous discussions in this section.

6.2 Rational Model

In this section we will derive expression of the Gaussian and mean curvatures of edge-vertex contact surfaces which arise when using the rational model for the configuration space. The case of vertex-edge contact is simpler and for the sake of brevity is omitted. Other geometrical properties, similar to those we derived in Section 6.1, can be derived as well.

From Equation (20) we have that a general edge-vertex contact surface is given by

$$S(t,\psi) = \begin{pmatrix} b_j - M^{\psi} \cdot a_{i,t} \\ \psi \end{pmatrix}$$

when modeling the configuration space using the rational model. It is easily shown that the partial derivatives are given by

$$\frac{\partial S}{\partial t} = \begin{pmatrix} -M^{\psi} \cdot (a_{i+1} - a_i) \\ 0 \end{pmatrix} \quad , \quad \frac{\partial S}{\partial \psi} = \begin{pmatrix} -\frac{d}{d\psi} M^{\psi} \cdot a_{i,t} \\ 1 \end{pmatrix}$$

In turn, the fundamental forms are given by

$$\begin{aligned} E &= \|a_i - a_{i+1}\|^2 & e &= 0 \\ F &= \frac{2}{1+\psi^2} \det(a_i, a_{i+1}) & f &= -\frac{2}{1+\psi^2} \frac{\|a_i - a_{i+1}\|^2}{\nu} \\ G &= 1 + \frac{4}{(1+\psi^2)^2} \|a_{i,t}\|^2 & g &= -\frac{4}{(1+\psi^2)^2} \frac{\det(a_i, a_{i+1}) + \psi \langle a_i - a_{i+1}, a_{i,t} \rangle}{\nu} \end{aligned}$$

Here, $\nu = \nu(t,\psi) = \sqrt{EG - F^2}$. Note that in contrast to the case discussed in Section 6.1, here ν depends on both t and ψ. Now, using the standard formulas for the Gaussian and mean curvatures, we can obtain the following expressions:

$$\begin{aligned} K(t,\psi) &= -\frac{4}{(1+\psi^2)^2} \frac{E^2}{\nu^4} \\ H(t,\psi) &= \frac{2E}{(1+\psi^2)\nu^3} \left(\frac{1}{2} F - \frac{\psi}{1+\psi^2} \langle a_i - a_{i+1}, a_{i,t} \rangle \right) \end{aligned}$$

In this case, when using the rational model, both curvatures depend on *both* parameters (cf. Equations (21) and (22) when using the geometric model). Note that

$$\begin{aligned} \lim_{t \to \pm\infty} K(t,\psi) &= \lim_{\psi \to \pm\infty} K(t,\psi) = 0 \\ \lim_{t \to \pm\infty} H(t,\psi) &= \lim_{\psi \to \pm\infty} H(t,\psi) = 0 \end{aligned}$$

7 Conclusion

In this report we discussed prominent aspects of the geometry of contact surfaces in the configuration space which arise when a planar convex polygon is free to translate and rotate amid planar polygonal obstacles. We considered two models of the configuration space, namely the geometrical one which is more intuitive and the rational one which is more suitable when machine-precision is needed. We started the discussion by providing an explicit and concise parameterizations for the surfaces that correspond to *vertex-edge* and *edge-vertex* contacts. Once the parameterizations were formulated we carried out standard differential geometry computations and derived (normally) compact expressions of important notions like the Gaussian and mean curvatures, principal curvatures and principal curvature directions, etc.

Application. Using the parameterization described in this paper we produced a short video [1] which visualizes the configuration space of a convex polygonal robot which moves amid convex polygonal obstacles in the plane. The video serves as an educational tool when studying the notion of configuration space.

Future work. The computations of the contact *patches* heavily rely on the assumption that the robot A is convex. Eliminating this restriction is of interest. Other interesting extensions of the parameterization would be to consider a robot with a boundary which consists of non-linear edges; for example circular arcs (cf. [17]).

Once the contact surfaces and patches can be explicitly parameterized, it is natural to consider their discretizations. An approximated version of the configuration space can be used to address the general problem of *motion planning*. Furthermore, given either the smooth or discrete representations of the contact surfaces or patches, it is possible to study their mutual intersections and their intersections with other elements in the configuration space, as done for example in [19]. This study can be of help in the investigation of the arrangement of the contact surfaces in the configuration space.

Acknowledgments. This work is part of the project *Computational Geometric Learning*. The project CG Learning acknowledges the financial support of the Future and Emerging Technologies (FET) program within the Seventh Framework Program for Research of the European Commission, under FET-Open grant number 255827.

A Angle Range Analysis Using Normals

In Section 3, given a contact type, we first parameterized the corresponding contact surface. Then, we found a sub-domain Φ for the parameter ϕ such that $S(t,\phi)_{|\phi\in\Phi}$ for $t \in (0,1)$ yielded the corresponding contact patch. The computations that we described in Sections 3.1.1 and 3.2.1 yielded explicit answers, which cannot be represented in an exact manner. In this section, we pose further assumptions on the setting of the robot,

and in turn we will be able to find the desired sub-domain without involving trigonometric functions. We discuss in this section both the vertex-edge and edge-vertex cases.

A.1 Vertex-Edge Case

Let i, j be two indices and consider the contact type (v_i-e_j) and let $S(t, \phi)$ be the corresponding contact type as given in Equation (9) for $t \in (0, 1)$ and $\phi \in [0, 2\pi)$. We want to find $\Phi \subset [0, 2\pi)$ such that for all $\phi \in \Phi$ we will have $A(\mathbf{q}_{a_i}(\phi))$ *touches* E_j^O. As we already saw, the sub-domain Φ does not depend on the point of contact on the edge E_j^O of the obstacle. Thus, for some fixed $t_0 \in (0, 1)$ let $\mathbf{q}_i(\phi) = S(t_0, \phi)$ be the helix which is contained in S and which corresponds to a pseudo contact between a_i and the point

$$P = P(t) = (1 - t_0)b_j + t_0 b_{j+1}$$

on the edge E_j^O of the obstacle O. We will find Φ for this single helix. More explicitly, for every ϕ we have that $a_i(\mathbf{q}_i(\phi))$ pseudo touches a fixed point P on the edge E_j^O. We want to find the values of ϕ for which $a_i(\mathbf{q}_i(\phi))$ will *touch* P.

In order to obtain the bounds on the angle ϕ for which $a_i(\mathbf{q}_i(\phi))$ merely touches P, we have to check the angles between the (inward) normals $\vec{n}_i^A, \vec{n}_{i-1}^A$ of the robot and $\vec{n}_j^O$ of the obstacle (cf. Figure 6). As both the robot and the obstacle are convex and we assume a counterclockwise order of their vertices, we can establish the following observation.

Observation 15. *The vertex $a_i(\mathbf{q}_i(\phi)$ touches the point $P \in E_j^O$ if and only if when traversing the circle of direction counterclockwise then the normals are ordered as follow $\vec{n}_{j-1}^A$, $-\vec{n}_j^O$ and $\vec{n}_j^A$.*

The condition in the observation can be expressed as the following system of inequalities:

$$\begin{cases} \det\left(\vec{n}_{i-1}^A(\mathbf{q}_i(\phi)), -\vec{n}_j^O\right) \geq 0 \\ \det\left(-\vec{n}_j^O, \vec{n}_i^A(\mathbf{q}_i(\phi))\right) \geq 0 \end{cases} \tag{27}$$

Here, as before, $\det(u, v)$ denotes the determinant of the 2×2 matrix formed by the two vectors u and v. Note that u, v need not be of unit length as we are merely interested in the sign of the determinant. This systems means that $\vec{n}_{i-1}^A(\mathbf{q}_i(\phi))$ and $-\vec{n}_j^O$ form a *right-turn* and the normal $-\vec{n}_j^O$ forms a *right-turn* with the normal $\vec{n}_i^A(\mathbf{q}_i(\phi))$ as well (see Figure 6).

For each $\phi \in [0, 2\pi)$ we have, using Equation (3), the following

$$a_{i\pm1}(\mathbf{q}_i(\phi)) = P - R^\phi a_i + R^\phi a_{i\pm1}.$$

In turn, the edge normals of the robot satisfy

$$\begin{aligned} \vec{n}_{i-1}^A(\mathbf{q}_i(\phi)) &= R^{\frac{\pi}{2}}(a_i(\mathbf{q}_i(\phi)) - a_{i-1}(\mathbf{q}_i(\phi)) \\ \vec{n}_i^A(\mathbf{q}_i(\phi)) &= R^{\frac{\pi}{2}}(a_{i+1}(\mathbf{q}_i(\phi)) - a_i(\mathbf{q}_i(\phi)) \end{aligned}$$

Since the normal $-\vec{n}_j^O$ is stationary, and does not depend on the configuration space we refer to it as a constant vector, where $-\vec{n}_j^O = (\cos\beta_j, \sin\beta_j)$, for some fixed $\beta_j \in [0, 2\pi)$. The system of inequalities from Equation (27) reduces to the following system

$$\begin{cases} r_{i-1}\cos(\phi + \alpha_{i-1} - \beta_j) - r_i \cos(\phi + \alpha_i - \beta_j) \geq 0 \\ -r_i \cos(\phi + \alpha_i - \beta_j) + r_{i+1}\cos(\phi + \alpha_{i+1} - \beta_j) \geq 0 \end{cases} \tag{28}$$

Although we obtained here a rather compact system of inequalities, it is, in general, hard to analytically reduce it further, and obtain the desired domain for ϕ. However, assuming $r_j = \text{const}$ for all j's, that is all the vertices of the robot lie on a circle of a fixed radius, we can use the *cosine difference* formula and reduce the system of inequalities further to obtain

$$\begin{cases} \sin\left(\dfrac{2\phi - 2\beta_j + \alpha_{i-1} + \alpha_i}{2}\right)\sin\left(\dfrac{\alpha_{i-1} - \alpha_i}{2}\right) \leq 0 \\ \sin\left(\dfrac{2\phi - 2\beta_j + \alpha_{i+1} + \alpha_i}{2}\right)\sin\left(\dfrac{\alpha_{i+1} - \alpha_i}{2}\right) \leq 0 \end{cases} \tag{29}$$

In this last system of inequalities both

$$\sin\left(\frac{\alpha_{i-1} - \alpha_i}{2}\right) \text{ and } \sin\left(\frac{\alpha_{i+1} - \alpha_i}{2}\right)$$

depend only on the properties of the robot and their sign can be easily found. Indeed, for $1 < i < n$ we have that $0 \leq \alpha_{i-1} \leq \alpha_i < 2\pi$ and in turn $\sin\frac{\alpha_{i-1}-\alpha_i}{2} \leq 0$. On the other hand, since $0 < \alpha_i \leq \alpha_{i+1} < 2\pi$ we have that $\sin\frac{\alpha_{i+1}-\alpha_i}{2} \geq 0$. Thus, the inequality in (29) holds if ϕ satisfies the following constrains.

Condition 16 $(1 < i < n)$**.**

$$\begin{cases} \beta_j - \dfrac{\alpha_{i-1} + \alpha_i}{2} \leq \phi \leq \pi + \beta_j - \dfrac{\alpha_{i-1} + a_i}{2} \\ \pi + \beta_j - \dfrac{\alpha_{i+1} + \alpha_i}{2} \leq \phi \leq 2\pi + \beta_j - \dfrac{\alpha_{i+1} + \alpha_i}{2} \end{cases}$$

The cases $i = 1$ and $i = n$ have to be treated separately. That is, depending on the signs of $\sin\frac{\alpha_{i-1}-\alpha_i}{2}$ and $\sin\frac{\alpha_{i+1}-\alpha_i}{2}$ the inequalities can be reduced into a condition similar to the one obtained for $1 < i < n$.

Let us stress again that the compact and exact representation of the range of ϕ as described in Condition 16 is valid only if the three vertices a_{i-1}, a_i and a_{i+1} of the robot have the same distance from the reference point. In order to obtain a complete description of the contact patches using this approach, all the vertices of the robot have to lie on a circle of some fixed radius. If the vertices do not lie on a circle, then the approach described in Section 3.1 can be used.

Before ending this section, let us consider Equation (28) again. The condition that we posed in order to solve that system, namely $r_j = \text{const}$ for all j's, is very restrictive.

Note, that for a given (v_i-e_j) contact it is enough to assume that $r_{i-1} = r_i = r_{i+1}$. Or, in other words, we can assume that a_{i-1}, a_i and a_{i+1} lie on a circle centered at R_0. However, since the reference point can be chosen arbitrarily, we can set it at the center of the circle defined by a_{i-1}, a_i and a_{i+1}. The problem with this approach is that the configuration space depends on the choosing of the reference point. Differently said, this approach will yield a domain of ϕ which *depends* on the specially chosen reference point. Applying this approach to a different contact, will yield a domain of ϕ which will be correct only for the corresponding configurations space. It might be possible to correct this, and "translate" the yielded domain from one configuration space to another.

A.2 Angle Range Analysis Using Normals - Edge-Vertex

As in the (v-e) contact case, here as well, we introduce an obstacle O and we rotate A such that its boundary point $a_{i,t} = (1-t)a_i + a_{i+1}$ is fixed to the obstacle's vertex b_j. We will now find the range of ϕ for which this pseudo contact is merely a contact. Formally, for some fixed t_0 this means that we will find the ϕ's for which $\mathbf{q}_i(\phi) = S(t_0, \phi)$ is in $\mathcal{C}_{\text{free}}$ and $S(\cdot,\cdot)$ is the surface defined in Equation (13). Like before, due to the consistent ordering of the vertices and the convexity of the objects the desired free configuration is obtained when $\vec{n}_i^A$ is between $-\vec{n}_{j-1}^O$ and $-\vec{n}_j^O$. Equivalently, when $-\vec{n}_{j-1}^O$ forms a *right-turn* with $\vec{n}_i^A$ and $\vec{n}_i^A$ forms another *right-turn* with $-\vec{n}_j^O$ (see Figure 7). Thus, in order to maintain a *contact* between E_i^A and the vertex b_j of the obstacle, the angle parameter ϕ has satisfy the following system of inequalities:

$$\begin{cases} \det\left(-\vec{n}_{j-1}^O, \vec{n}_i^A(\mathbf{q}_i(\phi))\right) \geq 0 \\ \det\left(\vec{n}_i^A(\mathbf{q}_i(\phi)), -\vec{n}_j^O\right) \geq 0 \end{cases}$$

For the sake of simplicity, we assume that $-\vec{n}_{j-1}^O = (\cos\beta_{j-1}, \sin\beta_{j-1})$ and $-\vec{n}_j^O = (\cos\beta_j, \sin\beta_j)$ for some fixed β_{j-1} and β_j. In addition, we have that

$$\vec{n}_i^A(\mathbf{q}_i(\phi) = R^{\phi+\frac{\pi}{2}} \cdot (a_{i+1} - a_i).$$

In turn, the system of inequalities reduces to

$$\begin{cases} r_i\cos(\alpha_i - \beta_{j-1} + \phi) - r_{i+1}\cos(\alpha_{i+1} - \beta_{j-1} + \phi) \geq 0 \\ -r_i\cos(\alpha_i - \beta_j + \phi) + r_{i+1}\cos(\alpha_{i+1} - \beta_j + \phi) \geq 0 \end{cases}$$

Next, assuming that $r_i = r_{i+1} > 0$, the last system of inequalities reduces to:

$$\begin{cases} \sin(\phi - \beta_{j-1} + \dfrac{\alpha_i + \alpha_{i+1}}{2})\sin\dfrac{\alpha_i - \alpha_{i+1}}{2} \leq 0 \\ \sin(\phi - \beta_j + \dfrac{\alpha_i + \alpha_{i+1}}{2})\sin\dfrac{\alpha_{i+1} - \alpha_i}{2} \leq 0 \end{cases}$$

Depending on i, the signs of $\sin\frac{\alpha_i - \alpha_{i+1}}{2}$ and $\sin\frac{\alpha_{i+1} - \alpha_i}{2}$ can be determined. In turn, the system of inequalities can be reduced and an expression for the range of ϕ can be obtained in a similar way to the one detailed in Appendix A.1.

B Differential Geometry of V-E Contact Surfaces

In general a vertex-edge contact surface is given by the parameterization in Equation (9). One can easily compute the first fundamental forms of this surface, namely

$$\begin{aligned} E &= \|E_j^O\|^2 \\ F &= -\left\langle E_j^O, R^{\phi+\frac{\pi}{2}} a_i \right\rangle \\ G &= 1 + \|a_i\|^2 \end{aligned} \tag{30}$$

Next, the surface normal is given by

$$\mathcal{N}(t,\phi) = \frac{1}{\sqrt{\|b_{j+1}-b_j\|^2 + \left\langle \cos\phi\, a_i + \sin\phi\, R^{\frac{\pi}{2}} a_i, b_{j+1}-b_j \right\rangle}} \begin{pmatrix} R^{-\frac{\pi}{2}}\,(b_{j+1}-b_j) \\ -\left\langle \cos\phi\, a_i + \sin\phi\, R^{\frac{\pi}{2}} a_i, b_{j+1}-b_j \right\rangle \end{pmatrix}$$

In turn, we can find expressions of the second fundamental forms, namely

$$\begin{aligned} e &= 0 \\ f &= 0 \\ g &= \frac{\left\langle \cos\phi\, R^{\frac{\pi}{2}} a_i - \sin\phi\, a_i, E_j^O \right\rangle}{\sqrt{\|E_j^O\|^2 + \left\langle \cos\phi\, a_i + \sin\phi\, R^{\frac{\pi}{2}} a_i, E_j^O \right\rangle^2}} \end{aligned} \tag{31}$$

It is now easy, using the formula given in Equation (21), to verify that the Gaussian curvature of a vertex-edge contact surface vanishes; that is such a surface is developable. One can next use the standard formula of the mean curvature, as can be found in Equation (22). The resulting expression is rather complicated, and of little interest, however, its numerator can be expressed as follows

$$\|E_j^O\|^2 \left\langle E_j^O, R^{\phi+\frac{\pi}{2}} a_i \right\rangle .$$

Since the edges of the obstacles are not degenerated, we can conclude that the mean curvature is identically zero if and only if $a_i = \vec{0}$. In this case, it is easily seen, from the parameterization of the contact surface directly, that the surface is a plane.

References

[1] Dror Atariah and Günter Rote. "Configuration space visualization". In: *Proceedings of the 2012 symposium on Computational Geometry*. SoCG '12. Chapel Hill, North Carolina, USA: ACM, 2012, pp. 415–416. ISBN: 978-1-4503-1299-8. DOI: 10.1145/2261250.2261313. URL: http://youtu.be/SBFwgR4K1Gk.

[2] Chanderjit Bajaj and Myung-Soo Kim. "Generation of Configuration Space Obstacles: Moving Algebraic Surfaces". In: *The International Journal of Robotics Research* 9.1 (1990), pp. 92–112. DOI: 10.1177/027836499000900104.

[3] Jean-Daniel Boissonnat and Francis Avnaim. *Polygon placement under translation and rotation*. Anglais. Rapport de recherche RR-0889. INRIA, 1988. URL: http://hal.inria.fr/inria-00075665/en/.

[4] R.C. Brost. "Computing metric and topological properties of configuration-space obstacles". In: *Proceedings of IEEE International Conference on Robotics and Automation, 1989*. 1989, 170–176 vol.1. DOI: 10.1109/ROBOT.1989.99985.

[5] Manfredo P. do Carmo. *Differential geometry of curves and surfaces*. Englewood Cliffs, N.J.: Prentice-Hall Inc., 1976, pp. viii+503.

[6] Howie Choset et al. *Principles of Robot Motion: Theory, Algorithms, and Implementations (Intelligent Robotics and Autonomous Agents series)*. The MIT Press, May 2005. ISBN: 9780262033275. URL: http://amazon.com/o/ASIN/0262033275/.

[7] Alfred Gray. *Modern Differential Geometry of Curves and Surfaces*. CRC Press, 1993.

[8] L Guibas and R Seidel. "Computing convolutions by reciprocal search". In: *Proceedings of the second annual symposium on Computational geometry*. SCG '86. Yorktown Heights, New York, USA: ACM, 1986, pp. 90–99. ISBN: 0-89791-194-6. DOI: 10.1145/10515.10525.

[9] Yong K. Hwang and Narendra Ahuja. "Gross motion planning – A survey". In: *ACM Comput. Surv.* 24.3 (Sept. 1992), pp. 219–291. ISSN: 0360-0300. DOI: 10.1145/136035.136037.

[10] S. Hyde et al. *The Language of Shape: The Role of Curvature in Condensed Matter: Physics, Chemistry and Biology*. Elsevier Science, 1996. ISBN: 9780080542546. URL: http://books.google.de/books?id=1LZlSZ7ORrQC.

[11] M.B. Ignat'ev, F.M. Kulakov, and A.M. Pokrovskiĭ. *Robot-manipulator control algorithms*. Joint Publications Research Service, 1973. URL: http://books.google.de/books?id=-PUqAQAAIAAJ.

[12] Jean-Claude Latombe. *Robot Motion Planning*. 3rd. Kluwer Academic Publishers, 1993.

[13] Jean-Paul Laumond, ed. *Robot Motion Planning and Control*. Lectures Notes in Control and Information Sciences. Springer, 1998.

[14] S. M. LaValle. *Planning Algorithms*. Cambridge, U.K.: Cambridge University Press, 2006.

[15] Tomás Lozano-Pérez and Michael A. Wesley. "An algorithm for planning collision-free paths among polyhedral obstacles". In: *Commun. ACM* 22.10 (Oct. 1979), pp. 560–570. ISSN: 0001-0782. DOI: 10.1145/359156.359164.

[16] Mikola Lysenko, Saigopal Nelaturi, and Vadim Shapiro. "Group morphology with convolution algebras". In: *Symposium on Solid and Physical Modeling*. 2010, pp. 11–22.

[17] Victor Milenkovic, Elisha Sacks, and Steven Trac. "Robust Complete Path Planning in the Plane". In: *Algorithmic Foundations of Robotics X*. Ed. by Emilio Frazzoli et al. Vol. 86. Springer Tracts in Advanced Robotics. Springer Berlin Heidelberg, 2013, pp. 37–52. ISBN: 978-3-642-36278-1. DOI: 10.1007/978-3-642-36279-8_3.

[18] Helmut Pottmann and Johannes Wallner. *Computational Line Geometry*. Springer-Verlag New York, Inc., 2001. ISBN: 3540420584.

[19] Oren Salzman et al. "Motion Planning via Manifold Samples". In: *ESA*. 2011, pp. 493–505.

[20] J.T. Schwartz and M. Sharir. "On the piano movers' problem: I. The case of a two-dimensional rigid polygonal body moving amidst polygonal barriers". In: *Communications on Pure and Applied Mathematics* 36 (1983), pp. 345–398.

[21] Bruno Siciliano and Oussama Khatib, eds. *Springer Handbook of Robotics*. 1st ed. Springer, June 2008. ISBN: 9783540239574. URL: http://amazon.com/o/ASIN/354023957X/.

[22] Justin Stoecker and Victor Milenkovic. "Interactive visualization of 3D configuration spaces". In: *Proceedings of the twenty-ninth annual symposium on Computational geometry*. SoCG '13. Rio de Janeiro, Brazil: ACM, 2013, pp. 341–342. ISBN: 978-1-4503-2031-3. DOI: 10.1145/2462356.2462358. URL: http://youtu.be/BsCcy0vYerw.

[23] Kai Tang and Yong-Jin Liu. "A geometric method for determining intersection relations between a movable convex object and a set of planar polygons". In: *Robotics, IEEE Transactions on* 20.4 (Aug. 2004), pp. 636–650. ISSN: 1552-3098. DOI: 10.1109/TRO.2004.829479.

[24] Gokul Varadhan. "Accurate sampling-based algorithms for surface extraction and motion planning". PhD thesis. Chapel Hill, NC, USA, 2005. ISBN: 0-542-48581-8.

[25] Gokul Varadhan et al. "Topology Preserving Approximation of Free Configuration Space". In: *International Conference on Robotics and Automation*. 2006, pp. 3041–3048. URL: http://gamma.cs.unc.edu/NOPATH/cspace.pdf.

[26] Kevin D. Wise and Adrian Bowyer. "A Survey of Global Configuration-Space Mapping Techniques for a Single Robot in a Static Environment". In: *The International Journal of Robotics Research* 19.8 (2000), pp. 762–779. DOI: 10.1177/02783640022067157.

[27] Elias K. Xidias, Philip N. Azariadis, and Nikos A. Aspragathos. "Path Planning of Holonomic and Non-Holonomic Robots Using Bump- Surfaces". In: *Computer-Aided Design and Applications* 5 (2008), pp. 497–507. URL: http://www.cadanda.com/CAD_5_1-4__497-507.pdf.